Supporting Information of

Nocturnal production of N_2O_5 and $ClNO_2$ in Delhi: driving factors and impacts

Yijing Chen[1,2], Cheng Wu[2]*, Epameinondas Tsiligiannis[2], Ravi Kant Pathak[2,3], Jan B. C. Pettersson[2], Harsh Raj Mishra[2,3]†, Gazala Habib[4], Geetam Tiwari[5], Kebin He[1], Jingkun Jiang[1]*, Mattias Hallquist[2]*

Affiliations:

[1]State Key Laboratory of Regional Environment and Sustainability, School of Environment, Tsinghua University, School of Environment, Tsinghua University; Beijing, 100084, China.

[2]Department of Chemistry and Molecular Biology, University of Gothenburg; Gothenburg, 40530, Sweden.

[3]Indo-Gangetic Plains Centre for Air Research and Education (IGP-CARE), Hamirpur, Uttar Pradesh, 210301, India.

[4]Transportation Research and Injury Prevention Centre, Indian Institute of Technology Delhi, New Delhi, 110016, India.

[5]Department of Civil Engineering, Indian Institute of Technology Delhi, New Delhi, 110016, India.

†Present address: School of Earth and Atmospheric Sciences, Queensland University of Technology, Queensland, 4001, Brisbane, Australia.

***Correspondence to:** Mattias Hallquist (hallq@chem.gu.se), Jingkun Jiang (jiangjk@tsinghua.edu.cn) and Cheng Wu (cheng.wu@gu.se).

This PDF file includes:

Text S1 to S3
Figures S1 to S20
Tables S1 to S3

Supplementary Text

Text. S1 Details of field measurements in Delhi

1.1 FIGAERO-I^--CIMS configurations

The reagent ions (I^- and $I \cdot H_2O^-$) were produced by passing ~2 lpm ultrahigh purity (UHP) N_2 via a CH_3I permeation tube and through a Po-210 ion source, where it interacted with the sampled air or thermally desorbed molecules from $PM_{2.5}$ in the ion-molecular reactor (IMR). A constant 10 sccm of H_2O-saturated UHP was added directly into the IMR to reduce the sensitivity variability with ambient RH. The IMR pressure was maintained at 200-250 mbar during gas sampling and 120-140 mbar during $PM_{2.5}$ desorption. The relatively lower pressure during the $PM_{2.5}$ measurement was likely caused by the resistance and associated pressure drop across the filters. Considering the differences in IMR pressures, we conducted sensitivity calibrations for the gas- and particle-phase measurements separately under conditions similar to the field observations in Delhi. The average mass resolution was ~3500 at m/z 127.

For the gas-phase measurements, ambient air was drawn at 3 lpm through a 4-m-long PFA tube (inner diameter, 5 mm, residence time 1.6 s) with 2 lpm pumped away, and the remaining 1 lpm was diluted with 1 lpm UHP N_2 before entering the IMR to avoid reagent ions titration by high levels of pollutants (e.g., HNO_3) in the ambient air. The inlet was flushed with ~2 lpm UHP N_2 during the first and last two minutes of each 20-min gas-phase measurement to obtain background signals, while ambient sampling was performed during the remaining period. The signals from the second zeroing period were used as the background, since those from the first zeroing period may have been influenced by carryover desorption signals (especially for sticky compounds) from the preceding particle-phase measurement (**Fig. S5**). The background-subtracted and dilution ratio (a factor of 2) corrected ion signals were subsequently averaged to 1-hour intervals. For $PM_{2.5}$ measurements, ambient air was drawn at 3 lpm through a 4-m-long copper tube (inner diameter, 5 mm) fitted with a $PM_{2.5}$ cyclone during the gas-sampling period, with 2 lpm discarded and 1 lpm collected on a Teflon filter for 20 min. The filter was then moved to the desorption position, where it was thermally desorbed and carried into the IMR under a 2 lpm flow of UHP N_2. The N_2 flow was gradually ramped from room temperature to 200 ℃ in 20 min, soaked at 200 ℃ for 20 min, and finally cooled back to room temperature in 10 min. The particle phase signal was integrated over the temperature ramping and soaking period during filter desorption. The baseline was determined from linear fitting of the signal between the onset of heating and the end of soaking and was integrated and subtracted from the integrated desorption signals.

1.2. Sensitivity calibrations of N_2O_5, $ClNO_2$ and related species

N_2O_5 and $ClNO_2$. N_2O_5 was prepared by mixing O_3 with excessive NO_2 to promote

the conversion of NO_3 to N_2O_5. The generated N_2O_5 concentrations were determined by the change in O_3 following the addition of NO_2, and different N_2O_5 levels was achieved via varying O_3 concentration (Bertram et al., 2009). The produced N_2O_5 was further diluted with humidified zero air to approximate Delhi RH conditions before entering the CIMS. $ClNO_2$ was produced by passing a known amount of N_2O_5 through a wetted NaCl-slurry placed in a Teflon tube, assuming a unit conversion from N_2O_5 to $ClNO_2$ (Finlayson-Pitts, 2003). All the tubings are covered by aluminum foil to avoid NO_3 photolysis and were flushed with dry zero air overnight before calibration to minimize potential N_2O_5 hydrolysis on the tubing surfaces. No water-dependent sensitivity correction was applied for N_2O_5 and $ClNO_2$, as no significant sensitivity variation was observed in the range of $H_2O{\cdot}I^-/I^-$ ratios during the field measurements in Delhi. The calibration curve for N_2O_5 and $ClNO_2$ are shown in **Fig. S19a-b.**

HCl and chloroacetic acid. A certified 10 ppm HCl gas cylinder (Linde Specialgas) was used as the standard source, which was diluted with zero air to different mixing ratios before introducing to the CIMS (**Fig. S19c**). Notably, we observed a significant decrease of the HCl sensitivity at high $H_2O{\cdot}I^-/I^-$ ratios (**Fig. S19d**), likely due to the competing effects of H_2O for clustering with iodide anion and that the reaction of HCl with $H_2O{\cdot}I^-$ is thermodynamically less favorable compared to reacting with iodide anion. The slight increase in HCl sensitivity with increasing $H_2O{\cdot}I^-/I^-$ ratio at low RH levels may be related to the stabilization of $HCl{\cdot}I^-$ clusters by water vapors. Similar patterns have been reported for other acids in a previous study (Lee et al., 2014). Gaseous chloroacetic acid was generated by placing solid chloroacetic acid in a glass vial submerged in a 30 °C water bath. The emission rate, determined by gravimetric weight loss analysis, was 177.3 ng/min. No significant H_2O dependence of chloroacetic acid sensitivity was observed.

Levoglucosan. A certain amount (10~90 ng) of levoglucosan dissolved in acetone solutions was deposited on the filter of the CIMS, and then the droplet underwent the same thermal desorption cycle as in the field measurements. The sensitivity for levoglucosan was derived as the integrated background-subtracted signals divided by the deposited mass.

1.3. Supporting measurements and data quality control

Meteorological factors, i.e., T, RH, wind speed, and wind direction, were measured by an automated weather station (AWS) (Davis Vantage Pro 2, Davis Instruments Corporation, USA). Trace gases, including O_3, NO and NO_2, CO, and SO_2 were measured by on-line gas analyzers (ECOTECH Serinus). For the long-term (2017~2024) hourly observation data obtained from R.K. Puram station, we applied rigorous quality

controls following recent studies (Vohra et al., 2025;Xie et al., 2024) with a few modifications, including (1) Remove duplicates: In sequences of five or more consecutive identical hourly values, only the first value out of the sequence is retained, (2) Remove outliers: For a 24-h running window, flag any observation as an outlier if its absolute difference from the median exceeds three times the Median Absolute Deviation (MAD, median distance between each observation and the median of all observations), (3) Remove constant data: In a 24-h running window, remove constant data values with coefficient of variation (ratio of standard deviation to the mean) less than 5%, (4) Validation of NO, NO_2 measurements by comparing with the measured NO_x: consider NO and NO_2 are reported correctly in unit of $\mu g/m^3$ and assess if NO_x calculated from these is within 2% of reported NO_x + 2.5 ppb. If not, the measured NO, NO_2, and NO_x data were omitted.

Text. S2 Estimation of the N_2O_5 uptake coefficient

2.1 Inapplicability of the steady-state method

The steady-state approximation of the NO_2-NO_3-N_2O_5 system is a widely applied method (Brown et al., 2003) for estimating the values for the NO_3 and N_2O_5 sinks (thereby $\gamma_{N_2O_5}$) in various atmospheric environments (Brown et al., 2006;Wang et al., 2017b;Wang et al., 2017a). This method assumes that production rate of NO_3 and N_2O_5 equals the sum of the loss rates during a certain period of the night (Eq. 1), and therefore k_{NO_3} and $k_{N_2O_5}$ can be determined as the slope and intercept, respectively, of the linear fitting between ${\tau_{N_2O_5}}^{-1}$ and $\frac{1}{K_{eq}[NO_2]}$ (Eq. 2). However, we found no siginificant positive even negative correlation between ${\tau_{N_2O_5}}^{-1}$ and $\frac{1}{K_{eq}[NO_2]}$ during the nighttime throughout the campaign (an example is shown in **Fig. S20**). This is likely attributed to the intense and variable NO_x emissions in Delhi (avg. nighttime hourly NO_x mixing ratios of 92±60 ppb) which preclude the system from approaching steady-state on the time-scale of a night. As is in shown in **Fig. 2a** of the main text, N_2O_5 presented a strong negative dependence on NO. The high concentrations and large flucuations of NO dominated the variation of N_2O_5, thereby decoupling the lifetime of N_2O_5 fro m $\frac{1}{K_{eq}[NO_2]}$.

$$k_{NO_2+O_3}[NO_2][O_3] = k_{NO_3}[NO_3] + k_{N_2O_5}[N_2O_5]\ (Eq.1)$$

$$K_{eq} = 2.7 \times 10^{-27} \times \exp(11000/T)$$

Substitute $[NO_3] = \frac{[N_2O_5]}{K_{eq}[NO_2]}$ to $Eq.1$, we get

$$\tau_{N_2O_5}{}^{-1} = \frac{k_{NO_2+O_3}[NO_2][O_3]}{[N_2O_5]} = \frac{k_{NO_3}}{K_{eq}[NO_2]} + k_{N_2O_5} \quad (Eq.2)$$

Where k_{NO_3} and $k_{N_2O_5}$ are the pseudo-first-order loss rate constants of NO_3 and N_2O_5, respectively, $k_{N_2O_5} = \frac{\bar{c}\gamma}{4} S_a$, $\tau_{N_2O_5}{}^{-1}$ is the inverse of the N_2O_5 steady-state liftime.

2.2 Validation of the RH parameterization method

$ClNO_2$ yield indicates the branching ratio of $H_2ONO_2^+$ reacting with H_2O (R4) and chloride (R5), which is theoretically determined by the respective reaction rates shown in Eq. 3(Bertram and Thornton, 2009).

$$f_{ClNO_2} = \frac{k_{R5}[H_2ONO_2^+][Cl^-]}{k_{R5}[H_2ONO_2^+][Cl^-] + k_{R4}[H_2ONO_2^+][H_2O]} = \frac{1}{1 + \frac{k_{R4}}{k_{R5}}\frac{[H_2O]}{[Cl^-]}} \quad (Eq.3)$$

Where $[H_2O]$ and $[Cl^-]$ are concentrations in the aqueous phase of particles derived from thermodynamic models, k_{R5} and k_{R4} are reaction rate coefficients of Reaction R5 and R4. The experimentally determined values for $\frac{k_{R5}}{k_{R4}}$ is 483±175 from the work of Bertram and Thornton(Bertram and Thornton, 2009) and 836±32 from Behnke et al(Behnke et al., 1997). Due to the lack of aerosol inorganic composition (e.g., NH_4^+, NO_3^-, and SO_4^{2-}) measurements during the 2023 campaign, we estimated the range of $[Cl^-]/[H_2O]$ ratio from January to March in 2022 Delhi when ACSM measurements are available(Ali et al., 2025) and the measured chloride level was similar to the campaign in 2023. The estimated nocturnal (18:00~06:00) $[Cl^-]/[H_2O]$ ratio ranged from 1.8×10^{-5} to 0.76 with an average of 0.07, which mostly fell in the region where the corresponding $ClNO_2$ yield close to 1 (**Fig. S13a**). We therefore tested the validity of the RH parameterization method by simulating the average nocturnal variation of $ClNO_2$ constrained with the parameterized gamma, observed N_2O_5 mixing ratios and aerosol surface area concentrations, with the $ClNO_2$ yield set to 1. The results showed that the simulation largely overestimated the production of $ClNO_2$ from 20:00 to 00:00 (**Fig. S13b**) when the absolute chloride concentrations were relatively low (**Fig. 1d**). By comparison, when constraining $ClNO_2$ yield to 0 for the chloride-deficient period (20:00 to 00:00) and 1 for the chloride-sufficient period (0:00 to 6:00), the modelled $ClNO_2$ evolution well tracked the observations (**Fig. S13b**). The overall consistency between modelling and observations suggest that the measured $ClNO_2$ can largely explained by the locally heterogeneous uptake of N_2O_5 on chloride-rich particles in Delhi and that the RH-parameterized $\gamma_{N_2O_5}$is a reasonable estimate, indicating the key role of RH and thereby aerosol liquid water content in driving N_2O_5 uptake in Delhi. Nevetheless, comprehensive aerosol composition measurements or direct

measurements of N_2O_5 reactivity (Bertram et al., 2009;Li et al., 2025) in future studies are required to enable better quantification and understanding N_2O_5 uptake processes in Delhi.

Text. S3 Estimation of $ClNO_2$ in the residual layer

The nocturnal boundary layer typically comprised a surface layer and an overlying residual layer (RL), where the RL was isolated from ground emissions and preserved the chemical composition of the well-mixed boundary layer from the late-afternoon. To estimate the maximum $ClNO_2$ produced in the RL, we used the ground-observed average N_2O_5 mixing ratios and aerosol surface area prior to sunset (16:00~18:00), assuming $\gamma_{N_2O_5}$=0.1 and f_{ClNO_2}=1 (Eq. 4). The calculation indicated that N_2O_5 was fully consumed within 1 hour.

$$[ClNO_2]_{RL} = \int_{t1}^{t2} \frac{\bar{c}\gamma_{N_2O_5}}{4} S_a [N_2O_5]_{obs} f_{ClNO_2}\, dt \quad \text{(Eq. 4)}$$

Table S1 Summary of nocturnal peak and average (shown in the brackets) N_2O_5 and $ClNO_2$ mixing ratios measured around the world. The unit is ppt.

Location	Period	Type	N_2O_5	$ClNO_2$	ref.
India Institute of Technology, Delhi	2023.2.23-3.14	urban inland	556 (16)	1340 (116)	this study
India Institute of Technology, Delhi	2019.1.11-2.5	urban inland	203 (4)	724 (48)	(Haslett et al., 2023)
Gulf of Mexico, Huston, Texas	2006.7-9	urban coastal	750	1200	(Osthoff et al., 2008)
National Oceanic and Atmospheric Administration, Boulder, Colorado	2009.2.11-2.25	urban inland	1500	440	(Thornton et al., 2010)
University of Utah, Salt Lake City, Utah	2015.12-2016.2	urban inland	1520 (76)		(Baasandorj et al., 2017)
University of Michigan, Ann Arbor, Michigan	2016.2.1-3.10	urban inland		220	(McNamara et al., 2020)
Toronto	2021.1.11-1.25	urban inland		300	(Wang et al., 2023)
Kensington	2012.7 -8	urban inland	1700	724 (84)	(Bannan et al., 2015)
Manchester	2014.10-11	urban inland		506	(Priestley et al., 2018)
Frankfurt Observatory (825 m a.s.l.)	2011.8-9	rural inland	3000	800	(Phillips et al., 2012)
China, Wangdu	2014.6-7	rural inland	500	2070	(Tham et al., 2016)
China, Wangdu	2017.12	rural inland	1000	1400	(Xia et al., 2021)
China, Wangdu	2023.2.10-3.5	rural inland		3600	(Chen et al., 2025)
China, mountain in Hong Kong (957 a.s.l.)	2013.11-12	mountain site	7700	4700	(Wang et al., 2016)
China, Heshan	2017.1.2-1.15	urban coastal	3000	8300	(Chen et al., 2023)

Table S2 Campaign-averaged NO_3· reactivity (unit: s^{-1}) during the 2019 and 2023 campaign.

	NO_3 + NO	NO_3 + hv	N_2O_5 hete.	NO_3 + VOCs
2019.1~2	50.175	0.031	0.462	0.081
2023.2~3	15.585	0.043	0.091	0.081*

*assumed to be the same as those observed in 2019.

Table S3 Average emission factor (g/kg fuel burned) of K, HCl, HCN, CO, and SO_2 from biomass, biofuel, and garbage burning processes and vehicles.

		K	HCl	HCN	SO_2	CO	HCl/CO	ref
Biomass burning	Peat	0.004~0.015	-	1.00	-	38	-	(Andreae, 2019)
	Crop residues	0.48	0.18	0.42	0.8	77	2.3×10^{-3}	(Andreae, 2019)
	Rice straw	-	0.44	0.37	1.3	60	7.3×10^{-3}	(Stockwell et al., 2014)
	Wheat straw	-	0.47	0.10	0.7	39	1.2×10^{-2}	(Stockwell et al., 2014)
	Tropical forest	0.32	0.13	0.44	0.8	104	1.3×10^{-3}	(Andreae, 2019)
	Temperate forest	0.18	0.04	0.64	0.7	112	3.5×10^{-4}	(Andreae, 2019)
Biofuel burning	Dung	0.09	0.04	1.30	0.7	89	4.3×10^{-4}	(Andreae, 2019)
	Biofuels without dung	0.13	0.08	0.39	0.5	84	8.9×10^{-4}	(Andreae, 2019)
	Charcoal	0.75	0.11	-	0.6	207	5.3×10^{-4}	(Andreae, 2019)
	Wood	-	0.02	0.54	bld	77	2.4×10^{-4}	(Stockwell et al., 2016)

Garbage burning	Garbage burning	0.02	2.80	0.43	0.5	66	4.2×10^{-2}	(Andreae, 2019)
	Mixed plastic garbage	-	2.30	0.43	bld	85	2.7×10^{-2}	(Stockwell et al., 2016)
Vehicles	Two-wheeled vehicles	-	bld	0.68	bld	761	-	(Stockwell et al., 2016)
	Agricultural diesel irrigation pumps	-	bld	0.12	bld	17	-	(Stockwell et al., 2016)

Note: bld indicates below the limit of detection.

Table S4 Summary of the bulk PM composition measured at IITD during winter from 2017 to 2022. The unit is μg/m^3.

Period	PM	Cl	NO_3	SO_4	NH_4	Org	ref
2017.1~2017.3	PM_1	14.2	16.1	15.8	15.7	81.0	(Gani et al., 2019)
2017.12~2018.3	PM_1	18.9	19.6	11.1	15.9	99.9	(Gani et al., 2019)
2018.1.17~1.19 2018.2.5~3.11	$PM_{2.5}$	20.4	13.3	12.0	14.3	65.3	(Lalchandani et al., 2021)
2019.1.11~2.5	PM_1	17.3	20.8	18.0	23.7	80.0	(Haslett et al., 2023)
2019.12.1~2020.1.5	$PM_{2.5}$	5.7	14.5	11.4	9.5	60.9	(Ali et al., 2023)
2020.2.1~3.20	PM_1	4.9	10.6	9.7	8.9	47.9	(Mandariya et al., 2024)
2020.12.15~12.31	$PM_{2.5}$	11.3	27.2	13.7	25.7	111.5	(Faisal et al., 2025)

2020.12.15~2021.2.23	$PM_{2.5}$	4.9	19.8	15.5	15.7	96.2	(Ali et al., 2023)
2021.1.1~2021.2.28	$PM_{2.5}$	10.1	16.1	12.1	19.0	87.0	(Faisal et al., 2025)
2022.1.12~3.31	$PM_{2.5}$	4.5	15.3	14.0	12.9	86.2	(Ali et al., 2025)

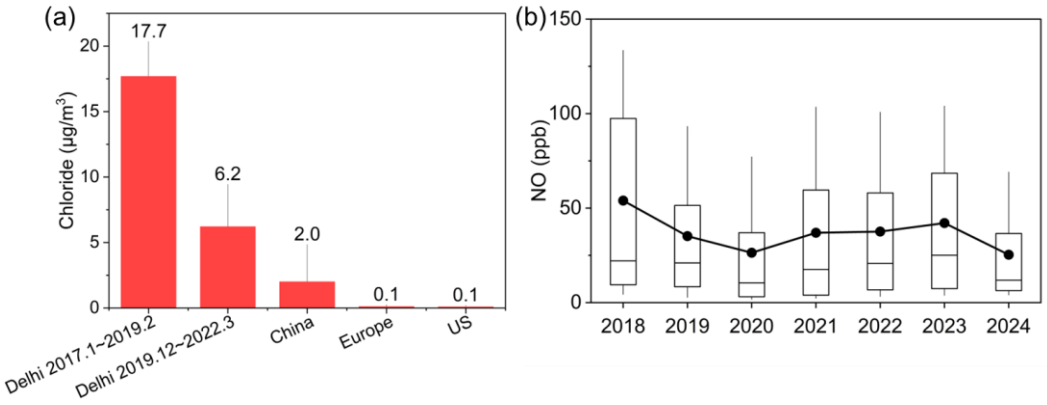

Fig. S1 (a) Comparison of the observed chloride levels globally. (b) Box plots of the annual daily averages of NO concentrations in Delhi. The chloride concentrations in Delhi (compiled from **Table S4**), China (Xia et al., 2021;Tham et al., 2018;Xia et al., 2020), Europe (Eger et al., 2019;Lanz et al., 2010), and US (Mielke et al., 2013;Sarwar et al., 2012) are campaign-average values retrieved from previous studies. The whiskers in (a) represent standard deviation. The NO concentrations shown in (b) were obtained from the R.K. Puram monitoring station. The boxes represent the interquartile range with the whiskers extending to the 10^{th} and 90^{th} percentiles. The dot and horizontal line within each box denote the mean and median values, respectively.

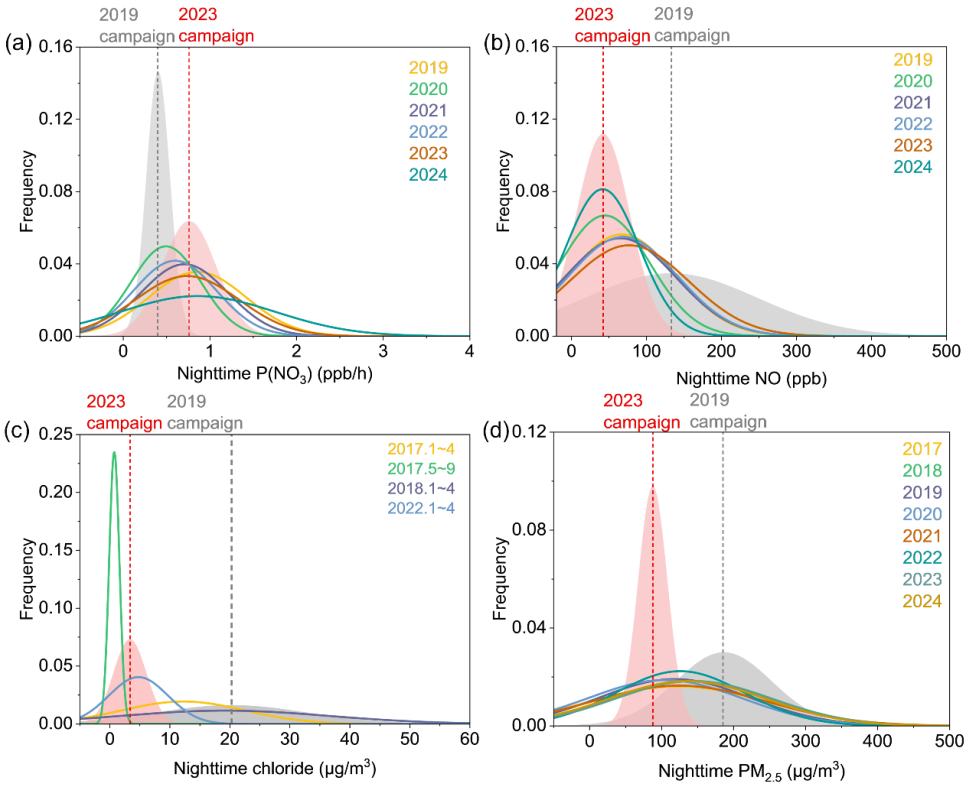

224

225 **Fig. S2 Representativeness of the two field-campaigns in Delhi.** Gaussian-fitted
226 frequency distributions of nightly (a) $P(NO_3)$, (b) NO, (c) chloride, and (d) $PM_{2.5}$
227 concentrations from 2017 to 2024. The nighttime is defined as 20:00~04:00 throughout
228 the years. The data for $P(NO_3)$, NO, and $PM_{2.5}$, are obtained from the R.K. Puram
229 monitoring station. Chloride concentrations were unavailable at the station and are
230 retrieved from previous studies (Gani et al., 2019;Ali et al., 2025). The gray and red
231 shaded area denote the respective pollutant distribution during the 2019 and 2023
232 campaign and the dashed lines indicate the campaign averages.

233

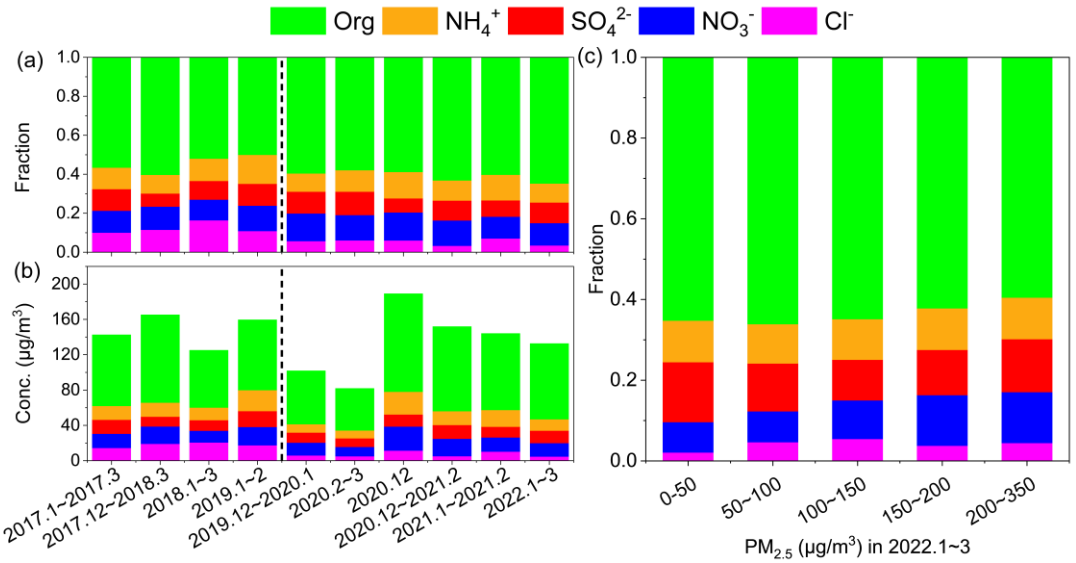

234

235 **Fig. S3 (a-b) Temporal trends in bulk PM composition measured at IITD during**
236 **winter from 2017 to 2022. (c) Variations of the composition fractions under**
237 **varying $PM_{2.5}$ ranges.** The original data for (a-b) was compiled from previous studies
238 based on ACSM or AMS measurements and shown in **Table S3**. The dashed vertical
239 line in (a-b) indicates the end of 2019. The $PM_{2.5}$ composition data in (c) was retrieved
240 from Ali et al(Ali et al., 2025). and the corresponding $PM_{2.5}$ mass concentrations were
241 obtained from the nearby R.K. Puram station.

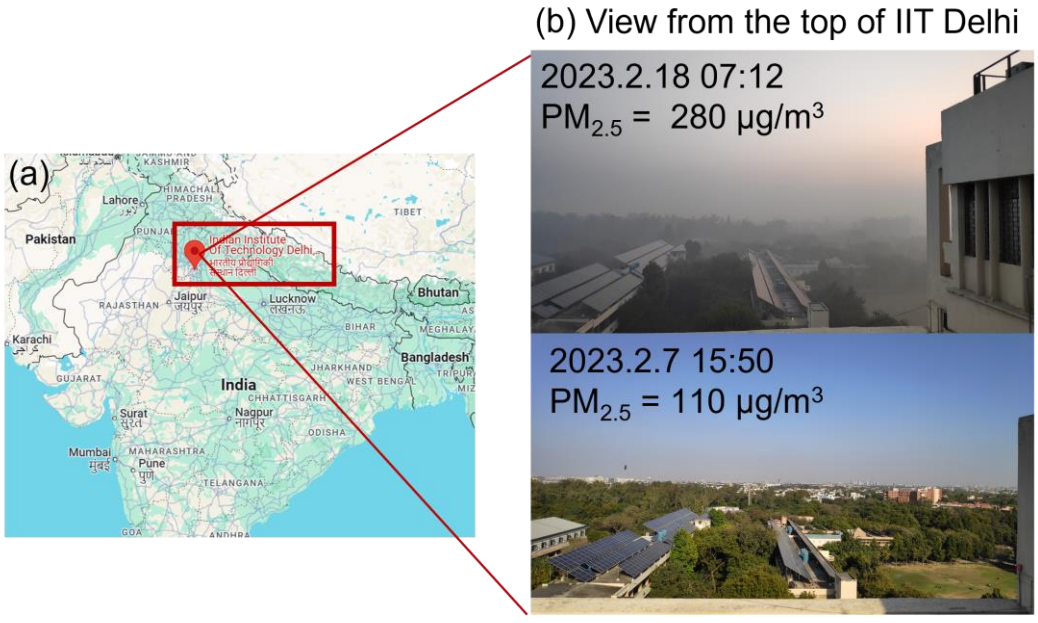

242

243 **Fig. S4 (a) The locations and (b) a zoom-in view of the sampling site**. The two photos
244 in (b) were taken during the early morning and late afternoon hours, respectively. Map
245 data © Google Maps 2026.

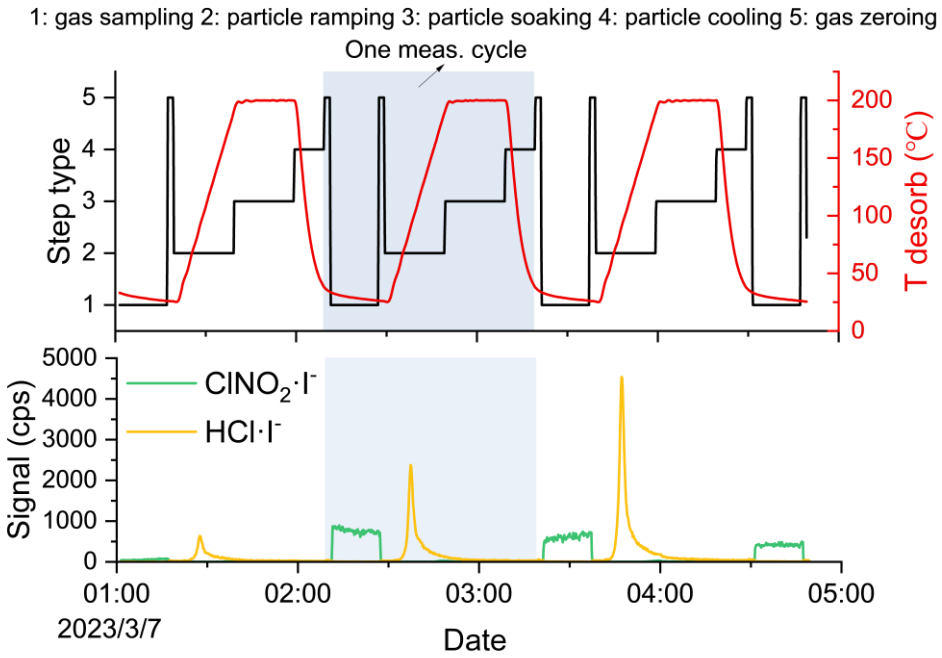

Fig. S5 An example of the measurement cycle.

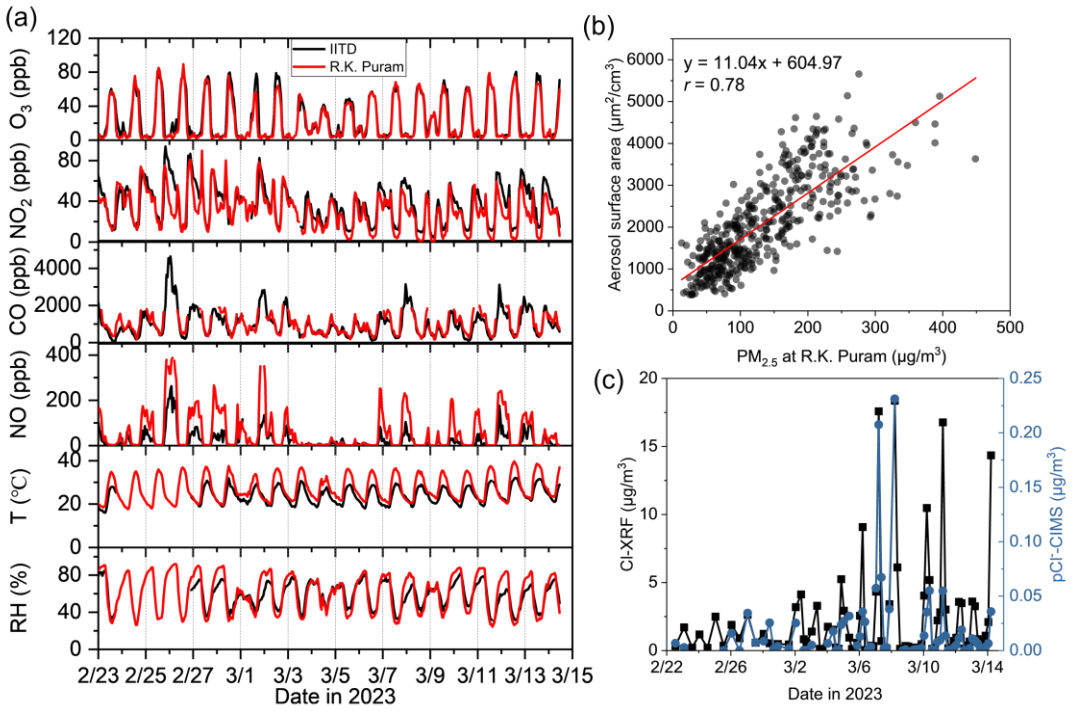

Fig. S6 Intercomparison of the measured species and estimation of aerosol surface area. (a) Comparison of the time series of trace gases and meteorological parameters measured at IIT Delhi and the R.K. Puram station in 2023 campaign. (b) Correlation between the measured aerosol surface area at IIT Delhi(Gani et al., 2020) and $PM_{2.5}$ at R.K. Puram station from February to March in 2018. (c) Time series of particulate Cl measured by XRF and CIMS.

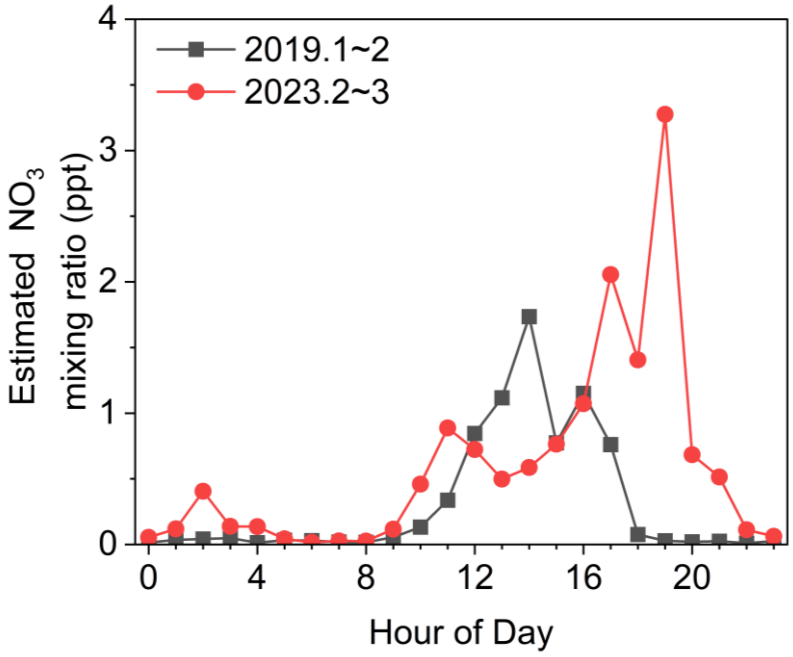

255

256 **Fig. S7 estimated NO_3· mixing ratios.** The NO_3 mixing ratio was estimated by using
257 the observed N_2O_5 and NO_2 mixing ratio and the temperature-dependent equilibrium
258 constant between NO_2, NO_3, and N_2O_5.

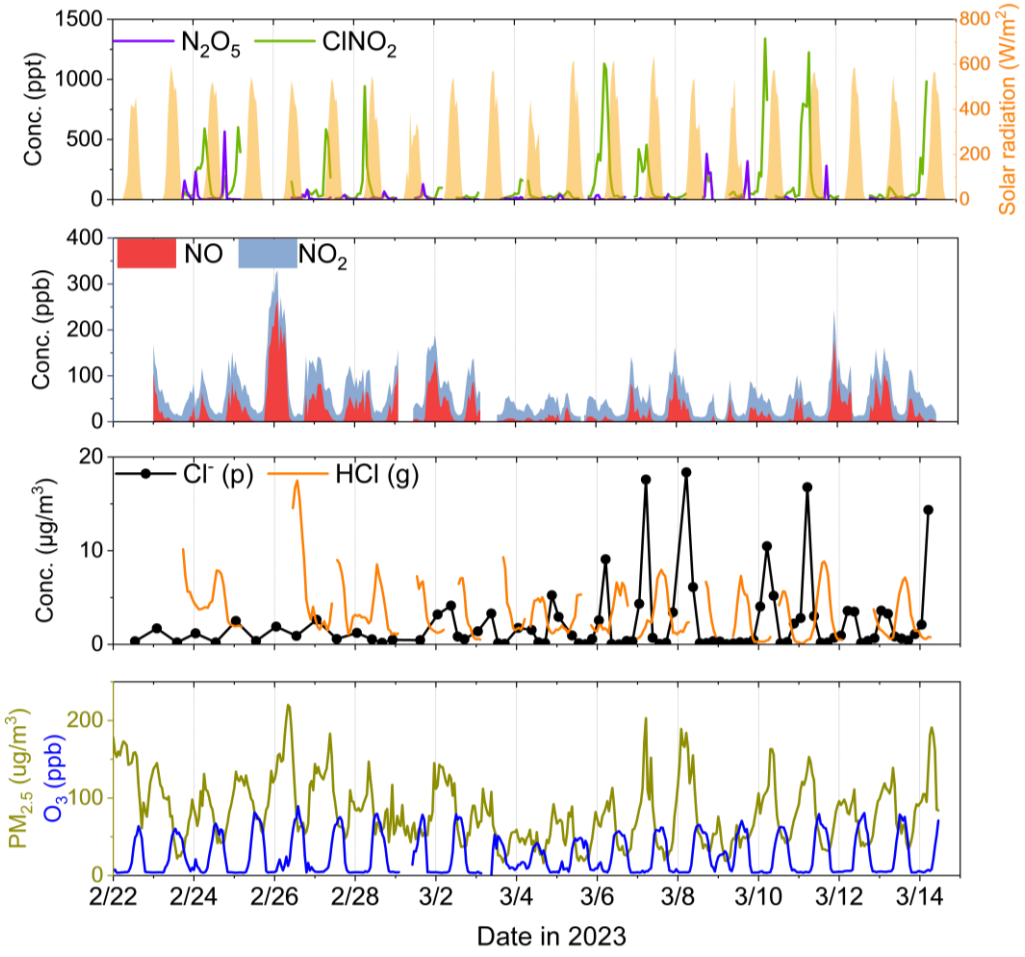

Fig. S8 Overview of the field observations. Time series of N_2O_5, $ClNO_2$, solar radiation, NO, NO_2, gaseous HCl, $PM_{2.5}$, and O_3, and Cl element concentrations in $PM_{2.5}$.

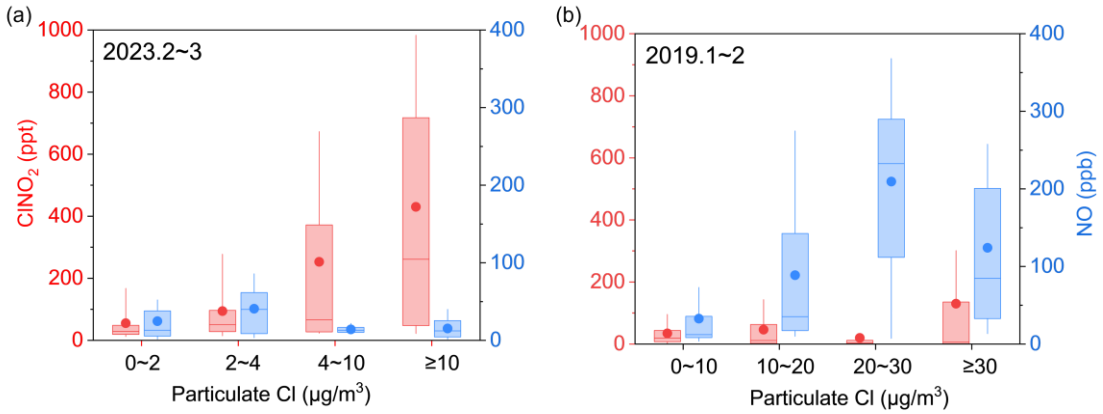

Fig. S9 Dependence of nocturnal $ClNO_2$ on chloride and NO during the (a) 2023 and (b) 2019 campaign. $ClNO_2$ and NO were stratified by chloride concentration intervals. Boxes and whiskers represent 25th and 75th , 10th and 90th percentiles, respectively. The dots and lines inside the box denote average and median values.

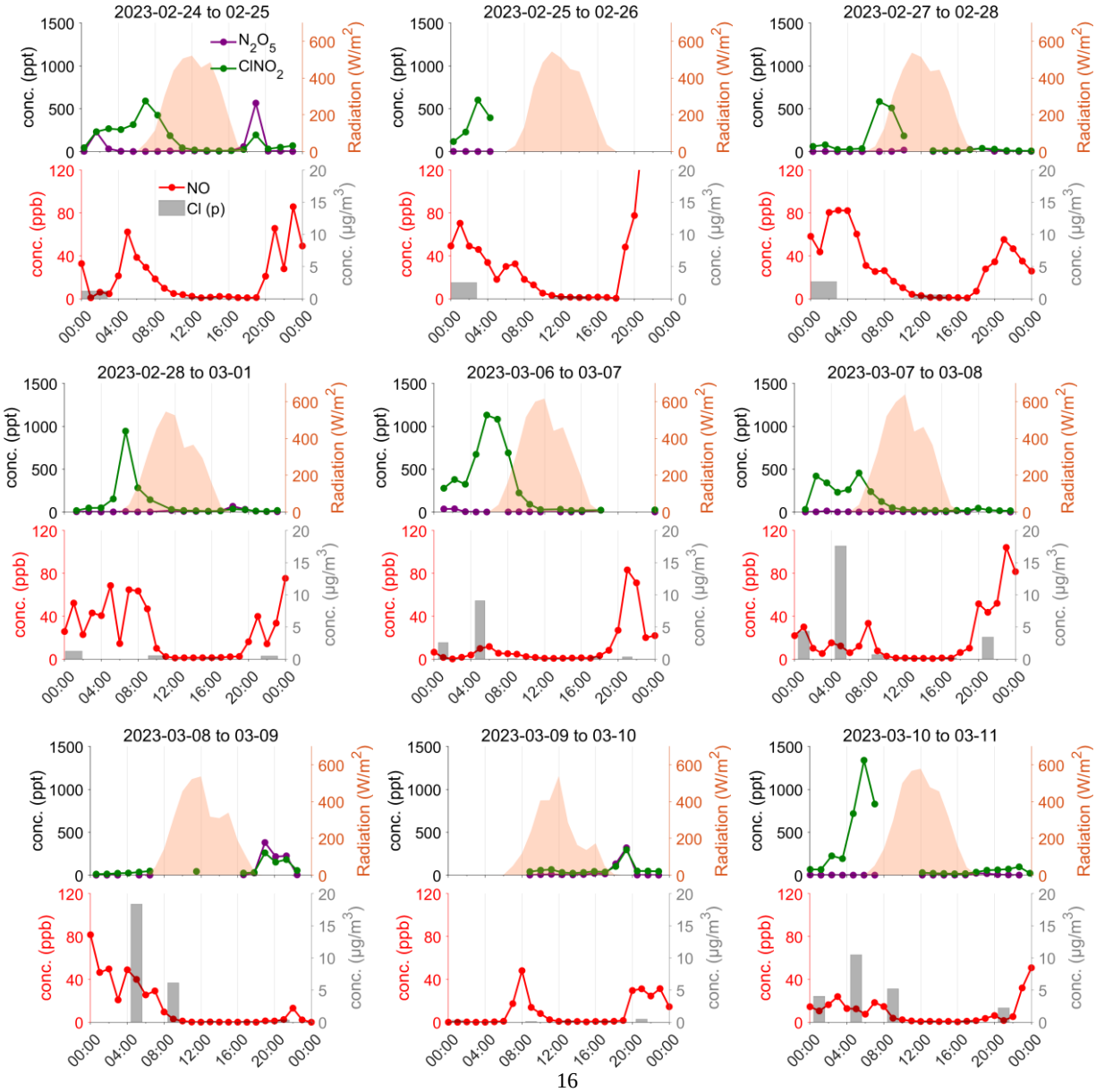

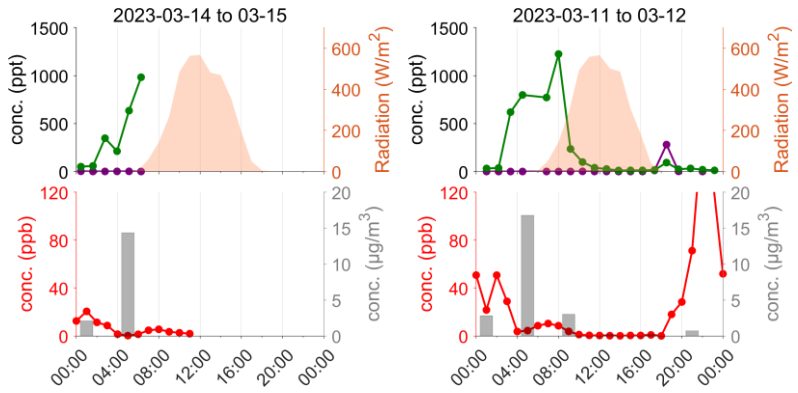

275 **Fig. S10 Day by day plots of the enhanced cases observed in 2023.** An enhanced
276 case is identified by a pronounced nighttime increase in either N_2O_5 or $ClNO_2$.
277

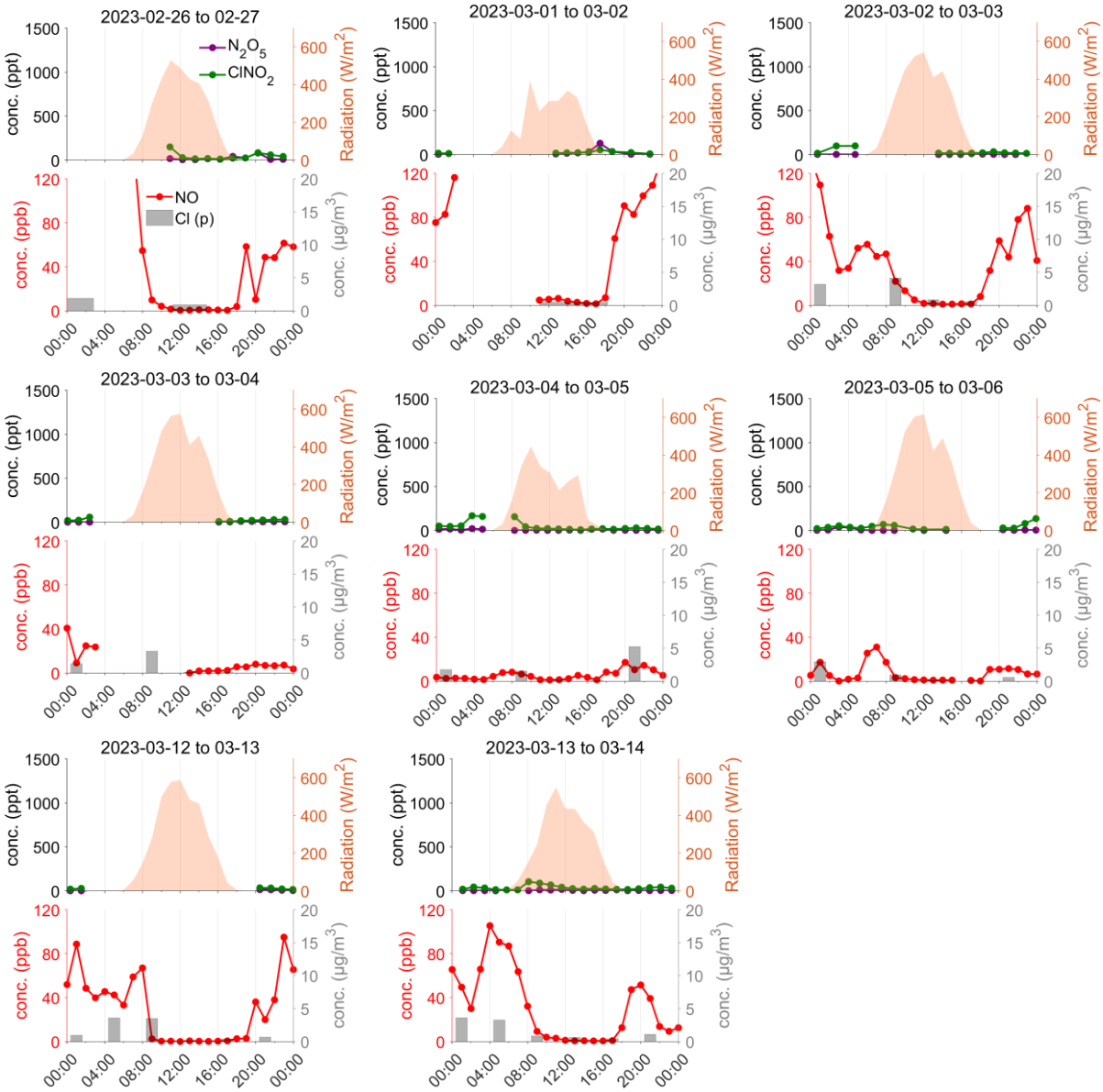

278

279 **Fig. S11 Day by day plots of the non-enhanced cases observed in 2023.** A non-

enhanced case is identified when neither N_2O_5 nor $ClNO_2$ shows a pronounced nighttime increase.

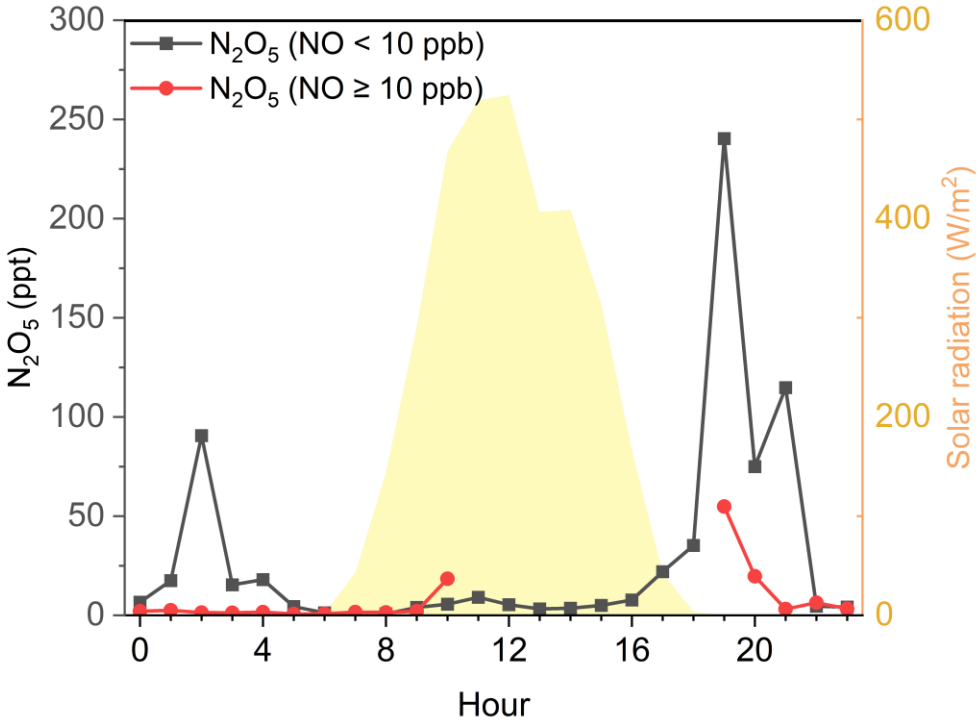

Fig. S12 Average diurnal variations of (a) N_2O_5 under low- and high-NO conditions (b) $PM_{2.5}$, total measured gaseous and particulate organics in 2023. A 10 ppb of NO threshold was applied to ensure statistically robust and comparable datasets. As all NO concentrations were below 10 ppb between 11:00 and 18:00, no N_2O_5 data are available for the high-NO condition during this period. The right axis in (b) shows the average solar radiation in 2023.

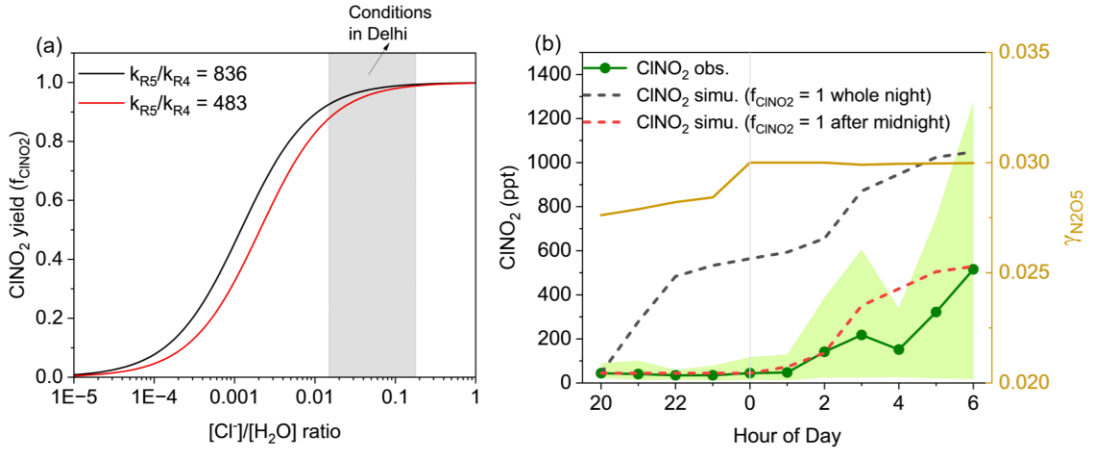

Fig. S13 (a) Parameterization of $ClNO_2$ yield and (b) simulation of the nocturnal $ClNO_2$ variations. The lines in (a) correspond to $ClNO_2$ yield calculated using Eq. 3 with different reported reaction rate constant ratios. The grey shaded area indicates the 10th and 90th percentiles of the calculated $[Cl^-]/[H_2O]$ ratios using ISOROPPIA from January to March of 2022 in Delhi(Ali et al., 2025). The green shaded area in (b) represents the 10th and 90th percentiles of the observed average nocturnal $ClNO_2$ mixing ratios. The dashed lines in (b) are the simulated $ClNO_2$ mixing ratios and the average RH parameterized N_2O_5 uptake coefficient is shown in the right axis of (b).

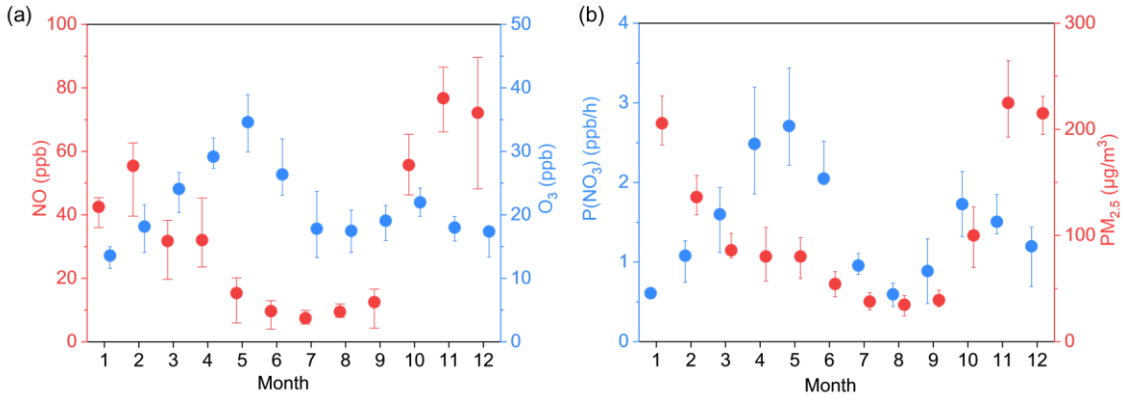

Fig. S14 Monthly variations of NO, O_3, $P(NO_3)$, and $PM_{2.5}$ in Delhi. Average monthly variations of (a) NO and O_3 and (b) $P(NO_3)$ and $PM_{2.5}$ from 2017 to 2024. The dots represent the averages and the whiskers denote the 25th to 75th percentile ranges. All data were obtained from the R.K. Puram national monitoring station.

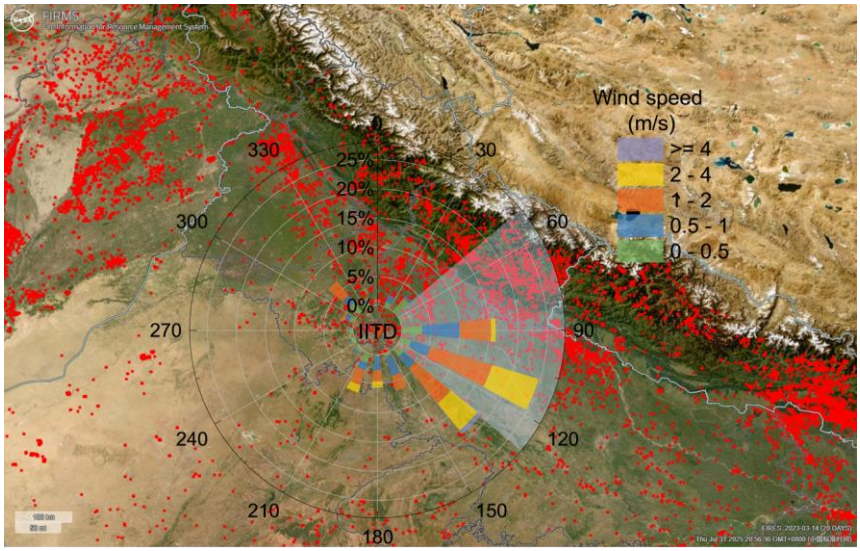

305

306 **Fig. S15 Satellite observations of active fire hotspots and wind rose plot during the**
307 **2023 campaign.** The map of the fire-points was downloaded from https://
308 earthdata.nasa.gov/firms. The measurement site (IIT Delhi) was indicated as IITD. The
309 light blue shaded area indicates the dominant wind-direction (50~130°) when the
310 extremely high values of the uptake parameter (γ×f) exceeding 0.1 were measured.

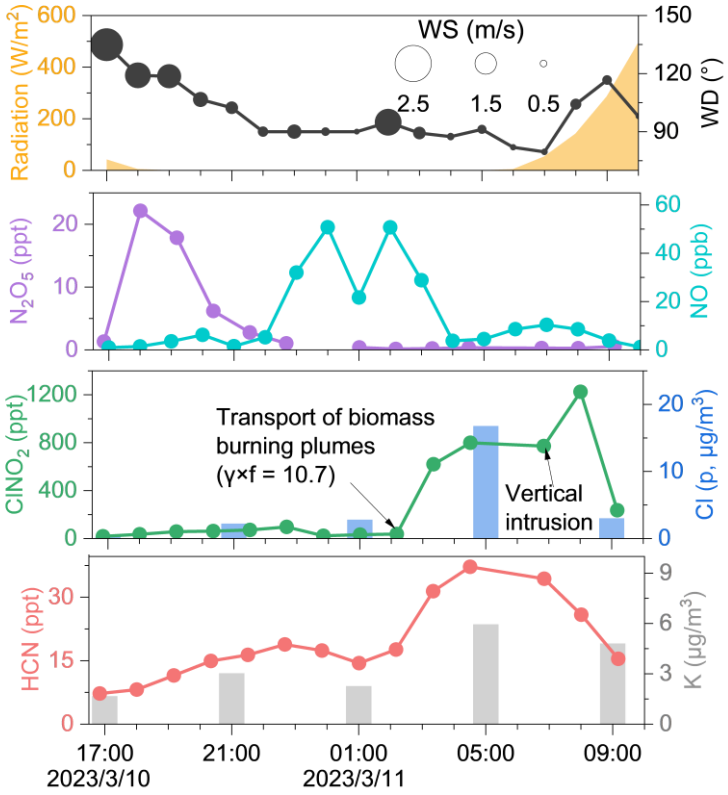

311

312 **Fig. S16 A case study indicating the influence of transport on the observed $ClNO_2$**
313 **levels.** An exceptionally high γ×f value (10.7) observed at 2023/3/11 2:10 is also noted.

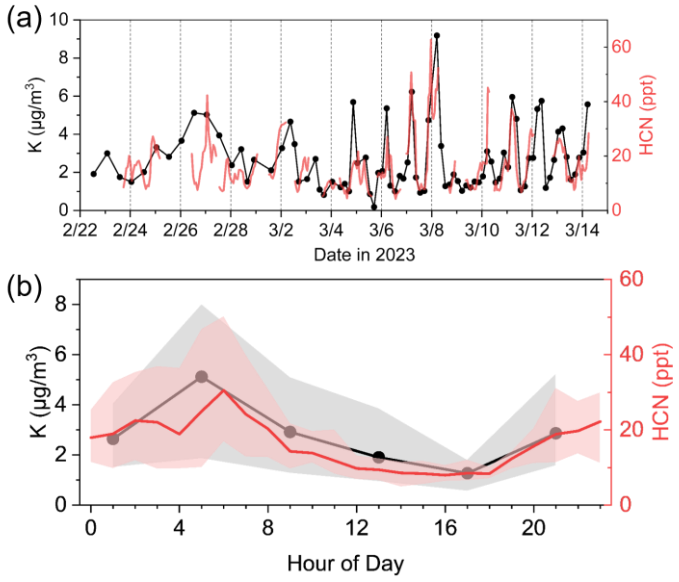

Fig. S17 (a) Time series and (b) average diurnal pattern of element K and gaseous HCN during the 2023 campaign. The shaded areas indicates 10th and 90th percentiles and the lines represent the campaign-averaged values. Hourly CIMS measurements were shown for HCN. The highest K and HCN concentrations on 3/7 and 3/8 were likely driven by large-scale bonfires involving wood and leaves burning during the Holika Dahan festival (3/6 16:00~3/8).

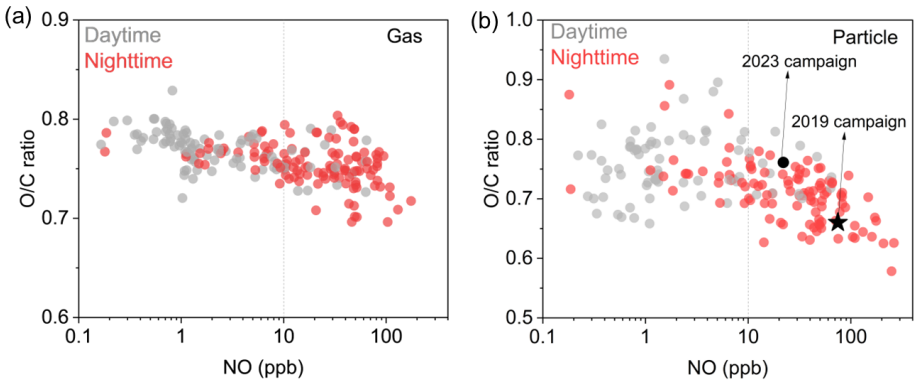

Fig. S18 NO dependence of the gaseous and particulate bulk O/C ratio in Delhi. Scatter plots showing the relationship between ambient NO levels and concentration-weighted bulk O/C ratios in the (a) gas and (b) particle phases.

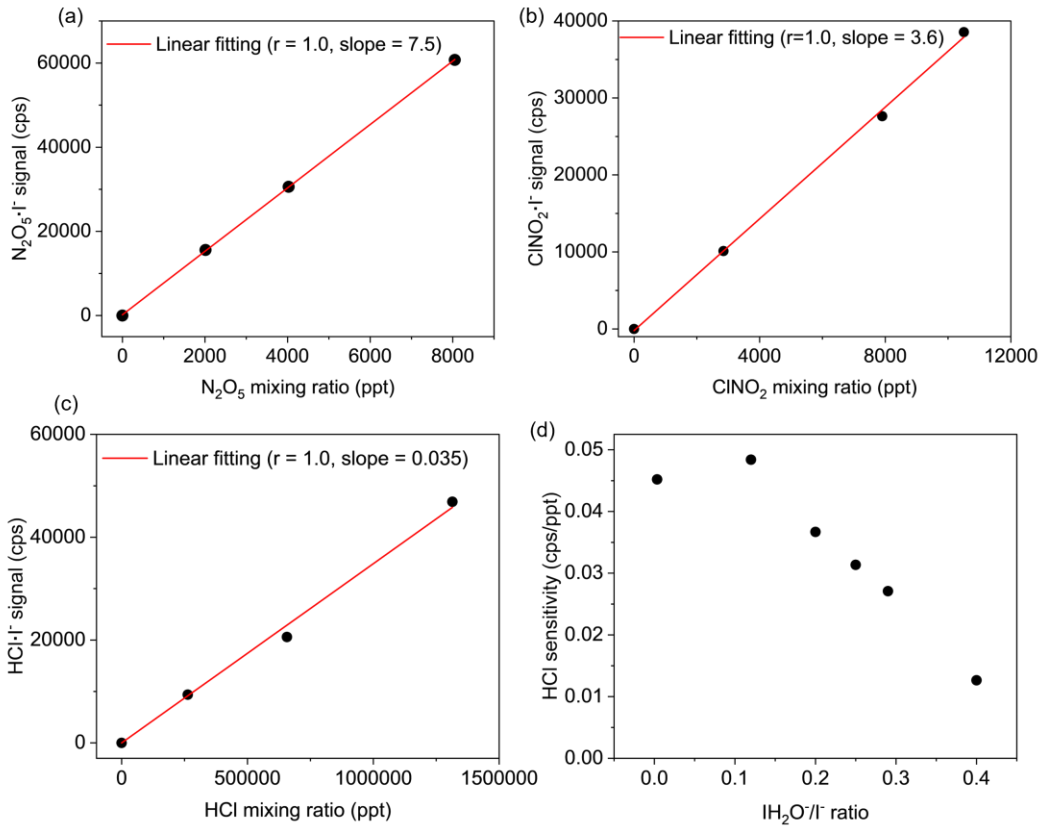

325

326 **Fig. S19 Sensitivity calibration of gaseous (a) N_2O_5, (b) $ClNO_2$, and (c) HCl and (d)**
327 **water dependency of HCl sensitivity.** Multi-point calibrations for N_2O_5 and $ClNO_2$
328 were performed under RH conditions corresponding to an IH_2O^- to I^- ratio of 0.42±0.02,
329 while the calibration curve at an $I{\cdot}H_2O^-$ to I^- ratio of 0.19 was shown for HCl.

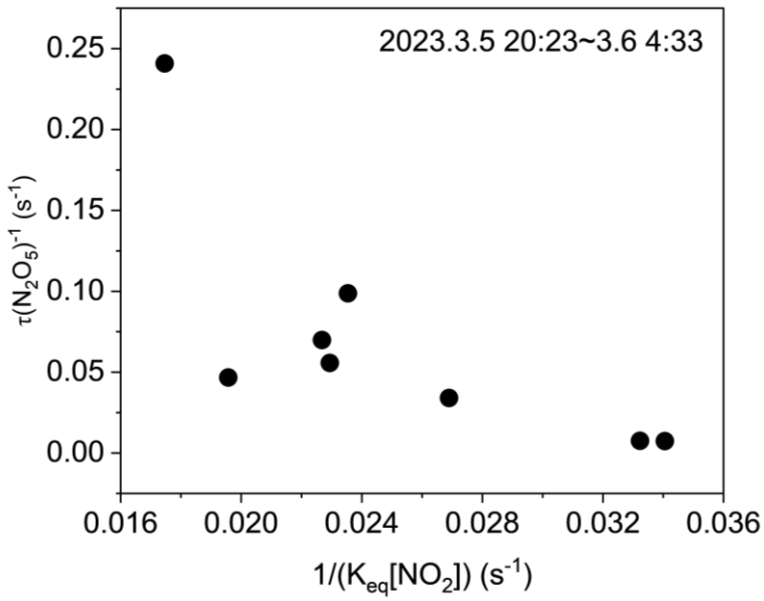

330

331 **Fig. S20 An example of the steady-state analysis of the NO_2-NO_3-N_2O_5 system.**

References

Ali, U., Faisal, M., Ganguly, D., Kumar, M., and Singh, V.: Analysis of aerosol liquid water content and its role in visibility reduction in Delhi, *Science of The Total Environment*, 867, 161484, https://doi.org/https://doi.org/10.1016/j.scitotenv.2023.161484, 2023.

Ali, U., Singh, V., Faisal, M., Kumar, M., and Gani, S.: Exploring the influence of physical and chemical factors on new particle formation in a polluted megacity, *Environmental Science: Atmospheres*, 5, 25-47, https://doi.org/10.1039/D4EA00114A, 2025.

Andreae, M. O.: Emission of trace gases and aerosols from biomass burning – an updated assessment, *Atmos. Chem. Phys.*, 19, 8523-8546, https://doi.org/10.5194/acp-19-8523-2019, 2019.

Baasandorj, M., Hoch, S. W., Bares, R., Lin, J. C., Brown, S. S., Millet, D. B., Martin, R., Kelly, K., Zarzana, K. J., Whiteman, C. D., Dube, W. P., Tonnesen, G., Jaramillo, I. C., and Sohl, J.: Coupling between Chemical and Meteorological Processes under Persistent Cold-Air Pool Conditions: Evolution of Wintertime $PM_{2.5}$ Pollution Events and N_2O_5 Observations in Utah's Salt Lake Valley, *Environmental Science & Technology*, 51, 5941-5950, https://doi.org/10.1021/acs.est.6b06603, 2017.

Bannan, T. J., Booth, A. M., Bacak, A., Muller, J. B. A., Leather, K. E., Le Breton, M., Jones, B., Young, D., Coe, H., Allan, J., Visser, S., Slowik, J. G., Furger, M., Prévôt, A. S. H., Lee, J., Dunmore, R. E., Hopkins, J. R., Hamilton, J. F., Lewis, A. C., Whalley, L. K., Sharp, T., Stone, D., Heard, D. E., Fleming, Z. L., Leigh, R., Shallcross, D. E., and Percival, C. J.: The first UK measurements of nitryl chloride using a chemical ionization mass spectrometer in central London in the summer of 2012, and an investigation of the role of Cl atom oxidation, *Journal of Geophysical Research: Atmospheres*, 120, 5638-5657, https://doi.org/10.1002/2014jd022629, 2015.

Behnke, W., George, C., Scheer, V., and Zetzsch, C.: Production and decay of ClNO2 from the reaction of gaseous N2O5 with NaCl solution: Bulk and aerosol experiments, *Journal of Geophysical Research: Atmospheres*, 102, 3795-3804, https://doi.org/https://doi.org/10.1029/96JD03057, 1997.

Bertram, T. H., and Thornton, J. A.: Toward a general parameterization of N_2O_5 reactivity on aqueous particles: the competing effects of particle liquid water, nitrate and chloride, *Atmos. Chem. Phys.*, 9, 8351-8363, https://doi.org/10.5194/acp-9-8351-2009, 2009.

Bertram, T. H., Thornton, J. A., and Riedel, T. P.: An experimental technique for the direct measurement of N_2O_5 reactivity on ambient particles, *Atmos. Meas. Tech.*, 2, 231-242, https://doi.org/10.5194/amt-2-231-2009, 2009.

Brown, S. S., Stark, H., and Ravishankara, A. R.: Applicability of the steady state approximation to the interpretation of atmospheric observations of NO3 and N2O5, *Journal of Geophysical Research: Atmospheres*, 108, https://doi.org/https://doi.org/10.1029/2003JD003407, 2003.

373 Brown, S. S., Ryerson, T. B., Wollny, A. G., Brock, C. A., Peltier, R., Sullivan, A. P.,
374 Weber, R. J., Dubé, W. P., Trainer, M., Meagher, J. F., Fehsenfeld, F. C., and
375 Ravishankara, A. R.: Variability in Nocturnal Nitrogen Oxide Processing and Its Role
376 in Regional Air Quality, *Science*, 311, 67-70,
377 https://doi.org/doi:10.1126/science.1120120, 2006.
378 Chen, X., Xia, M., Wang, W., Yun, H., Yue, D., and Wang, T.: Fast near-surface $ClNO_2$
379 production and its impact on O_3 formation during a heavy pollution event in South
380 China, *Sci Total Environ*, 858, 159998, https://doi.org/10.1016/j.scitotenv.2022.159998,
381 2023.
382 Chen, X., Jiang, Y., Zong, Z., Wang, Y., Sun, W., Wang, Y., Xia, M., Guan, L., Liu, P.,
383 Zhang, C., Chen, J., Mu, Y., and Wang, T.: Atmospheric Reactive Halogens Reshaped
384 by the Clean Energy Policy and Agricultural Activity in a Rural Area of the North China
385 Plain, *Environmental Science & Technology*, https://doi.org/10.1021/acs.est.4c13986,
386 2025.
387 Eger, P. G., Friedrich, N., Schuladen, J., Shenolikar, J., Fischer, H., Tadic, I., Harder,
388 H., Martinez, M., Rohloff, R., Tauer, S., Drewnick, F., Fachinger, F., Brooks, J.,
389 Darbyshire, E., Sciare, J., Pikridas, M., Lelieveld, J., and Crowley, J. N.: Shipborne
390 measurements of $ClNO_2$ in the Mediterranean Sea and around the Arabian Peninsula
391 during summer, *Atmospheric Chemistry and Physics*, 19, 12121-12140,
392 https://doi.org/10.5194/acp-19-12121-2019, 2019.
393 Faisal, M., Ali, U., Kumar, A., Kumar, M., and Singh, V.: Unveiling PM2.5 sources:
394 Double and tracer conjugate PMF approaches for high-resolution organic, BC, and
395 inorganic PM2.5 data, *Atmospheric Environment*, 343, 121011,
396 https://doi.org/https://doi.org/10.1016/j.atmosenv.2024.121011, 2025.
397 Finlayson-Pitts, B. J.: The Tropospheric Chemistry of Sea Salt: A Molecular-Level
398 View of the Chemistry of NaCl and NaBr, *Chemical Reviews*, 103, 4801-4822,
399 https://doi.org/10.1021/cr020653t, 2003.
400 Gani, S., Bhandari, S., Seraj, S., Wang, D. S., Patel, K., Soni, P., Arub, Z., Habib, G.,
401 Hildebrandt Ruiz, L., and Apte, J. S.: Submicron aerosol composition in the world's
402 most polluted megacity: the Delhi Aerosol Supersite study, *Atmos. Chem. Phys.*, 19,
403 6843-6859, https://doi.org/10.5194/acp-19-6843-2019, 2019.
404 Gani, S., Bhandari, S., Patel, K., Seraj, S., Soni, P., Arub, Z., Habib, G., Hildebrandt
405 Ruiz, L., and Apte, J. S.: Particle number concentrations and size distribution in a
406 polluted megacity: the Delhi Aerosol Supersite study, *Atmos. Chem. Phys.*, 20, 8533-
407 8549, https://doi.org/10.5194/acp-20-8533-2020, 2020.
408 Haslett, S. L., Bell, D. M., Kumar, V., Slowik, J. G., Wang, D. S., Mishra, S., Rastogi,
409 N., Singh, A., Ganguly, D., Thornton, J., Zheng, F., Li, Y., Nie, W., Liu, Y., Ma, W., Yan,
410 C., Kulmala, M., Daellenbach, K. R., Hadden, D., Baltensperger, U., Prevot, A. S. H.,
411 Tripathi, S. N., and Mohr, C.: Nighttime NO emissions strongly suppress chlorine and
412 nitrate radical formation during the winter in Delhi, *Atmos. Chem. Phys.*, 23, 9023-9036,
413 https://doi.org/10.5194/acp-23-9023-2023, 2023.
414 Lalchandani, V., Kumar, V., Tobler, A., M. Thamban, N., Mishra, S., Slowik, J. G.,

Bhattu, D., Rai, P., Satish, R., Ganguly, D., Tiwari, S., Rastogi, N., Tiwari, S., Močnik, G., Prévôt, A. S. H., and Tripathi, S. N.: Real-time characterization and source apportionment of fine particulate matter in the Delhi megacity area during late winter, *Science of The Total Environment*, 770, 145324, https://doi.org/https://doi.org/10.1016/j.scitotenv.2021.145324, 2021.

Lanz, V. A., Prévôt, A. S. H., Alfarra, M. R., Weimer, S., Mohr, C., DeCarlo, P. F., Gianini, M. F. D., Hueglin, C., Schneider, J., Favez, O., D'Anna, B., George, C., and Baltensperger, U.: Characterization of aerosol chemical composition with aerosol mass spectrometry in Central Europe: an overview, *Atmos. Chem. Phys.*, 10, 10453-10471, https://doi.org/10.5194/acp-10-10453-2010, 2010.

Lee, B. H., Lopez-Hilfiker, F. D., Mohr, C., Kurten, T., Worsnop, D. R., and Thornton, J. A.: An iodide-adduct high-resolution time-of-flight chemical-ionization mass spectrometer: application to atmospheric inorganic and organic compounds, *Environ Sci Technol*, 48, 6309-6317, https://doi.org/10.1021/es500362a, 2014.

Li, J., Zhai, T., Chen, X., Wang, H., Xie, S., Chen, S., Li, C., Gong, Y., Dong, H., and Lu, K.: Direct measurement of N_2O_5 heterogeneous uptake coefficients on atmospheric aerosols in southwestern China and evaluation of current parameterizations, *Atmos. Chem. Phys.*, 25, 6395-6406, https://doi.org/10.5194/acp-25-6395-2025, 2025.

Mandariya, A. K., Ahlawat, A., Haneef, M., Baig, N. A., Patel, K., Apte, J., Hildebrandt Ruiz, L., Wiedensohler, A., and Habib, G.: Measurement report: Hygroscopicity of size-selected aerosol particles in the heavily polluted urban atmosphere of Delhi: impacts of chloride aerosol, *Atmos. Chem. Phys.*, 24, 3627-3647, https://doi.org/10.5194/acp-24-3627-2024, 2024.

McNamara, S. M., Kolesar, K. R., Wang, S., Kirpes, R. M., May, N. W., Gunsch, M. J., Cook, R. D., Fuentes, J. D., Hornbrook, R. S., Apel, E. C., China, S., Laskin, A., and Pratt, K. A.: Observation of Road Salt Aerosol Driving Inland Wintertime Atmospheric Chlorine Chemistry, *ACS Cent Sci*, 6, 684-694, https://doi.org/10.1021/acscentsci.9b00994, 2020.

Mielke, L. H., Stutz, J., Tsai, C., Hurlock, S. C., Roberts, J. M., Veres, P. R., Froyd, K. D., Hayes, P. L., Cubison, M. J., Jimenez, J. L., Washenfelder, R. A., Young, C. J., Gilman, J. B., Gouw, J. A., Flynn, J. H., Grossberg, N., Lefer, B. L., Liu, J., Weber, R. J., and Osthoff, H. D.: Heterogeneous formation of nitryl chloride and its role as a nocturnal NO_x reservoir species during CalNex-LA 2010, *Journal of Geophysical Research: Atmospheres*, 118, 10638-10652, https://doi.org/10.1002/jgrd.50783, 2013.

Osthoff, H. D., Roberts, J. M., Ravishankara, A. R., Williams, E. J., Lerner, B. M., Sommariva, R., Bates, T. S., Coffman, D., Quinn, P. K., Dibb, J. E., Stark, H., Burkholder, J. B., Talukdar, R. K., Meagher, J., Fehsenfeld, F. C., and Brown, S. S.: High levels of nitryl chloride in the polluted subtropical marine boundary layer, *Nature Geoscience*, 1, 324-328, https://doi.org/10.1038/ngeo177, 2008.

Phillips, G. J., Tang, M. J., Thieser, J., Brickwedde, B., Schuster, G., Bohn, B., Lelieveld, J., and Crowley, J. N.: Significant concentrations of nitryl chloride observed in rural continental Europe associated with the influence of sea salt chloride and

anthropogenic emissions, *Geophysical Research Letters*, 39, n/a-n/a, https://doi.org/10.1029/2012gl051912, 2012.
Priestley, M., le Breton, M., Bannan, T. J., Worrall, S. D., Bacak, A., Smedley, A. R. D., Reyes-Villegas, E., Mehra, A., Allan, J., Webb, A. R., Shallcross, D. E., Coe, H., and Percival, C. J.: Observations of organic and inorganic chlorinated compounds and their contribution to chlorine radical concentrations in an urban environment in northern Europe during the wintertime, *Atmospheric Chemistry and Physics*, 18, 13481-13493, https://doi.org/10.5194/acp-18-13481-2018, 2018.
Sarwar, G., Simon, H., Bhave, P., and Yarwood, G.: Examining the impact of heterogeneous nitryl chloride production on air quality across the United States, *Atmos. Chem. Phys.*, 12, 6455-6473, https://doi.org/10.5194/acp-12-6455-2012, 2012.
Stockwell, C. E., Yokelson, R. J., Kreidenweis, S. M., Robinson, A. L., DeMott, P. J., Sullivan, R. C., Reardon, J., Ryan, K. C., Griffith, D. W. T., and Stevens, L.: Trace gas emissions from combustion of peat, crop residue, domestic biofuels, grasses, and other fuels: configuration and Fourier transform infrared (FTIR) component of the fourth Fire Lab at Missoula Experiment (FLAME-4), *Atmos. Chem. Phys.*, 14, 9727-9754, https://doi.org/10.5194/acp-14-9727-2014, 2014.
Stockwell, C. E., Christian, T. J., Goetz, J. D., Jayarathne, T., Bhave, P. V., Praveen, P. S., Adhikari, S., Maharjan, R., DeCarlo, P. F., Stone, E. A., Saikawa, E., Blake, D. R., Simpson, I. J., Yokelson, R. J., and Panday, A. K.: Nepal Ambient Monitoring and Source Testing Experiment (NAMaSTE): emissions of trace gases and light-absorbing carbon from wood and dung cooking fires, garbage and crop residue burning, brick kilns, and other sources, *Atmos. Chem. Phys.*, 16, 11043-11081, https://doi.org/10.5194/acp-16-11043-2016, 2016.
Tham, Y. J., Wang, Z., Li, Q., Yun, H., Wang, W., Wang, X., Xue, L., Lu, K., Ma, N., Bohn, B., Li, X., Kecorius, S., Größ, J., Shao, M., Wiedensohler, A., Zhang, Y., and Wang, T.: Significant concentrations of nitryl chloride sustained in the morning: investigations of the causes and impacts on ozone production in a polluted region of northern China, *Atmospheric Chemistry and Physics*, 16, 14959-14977, https://doi.org/10.5194/acp-16-14959-2016, 2016.
Tham, Y. J., Wang, Z., Li, Q., Wang, W., Wang, X., Lu, K., Ma, N., Yan, C., Kecorius, S., Wiedensohler, A., Zhang, Y., and Wang, T.: Heterogeneous N_2O_5 uptake coefficient and production yield of $ClNO_2$ in polluted northern China: roles of aerosol water content and chemical composition, *Atmos. Chem. Phys.*, 18, 13155-13171, https://doi.org/10.5194/acp-18-13155-2018, 2018.
Thornton, J. A., Kercher, J. P., Riedel, T. P., Wagner, N. L., Cozic, J., Holloway, J. S., Dube, W. P., Wolfe, G. M., Quinn, P. K., Middlebrook, A. M., Alexander, B., and Brown, S. S.: A large atomic chlorine source inferred from mid-continental reactive nitrogen chemistry, *Nature*, 464, 271-274, https://doi.org/10.1038/nature08905, 2010.
Vohra, K., S, M., Chakraborty, A., Shah, H., As, B., and Pakki, J.: Urgent issues regarding real-time air quality monitoring data in India: Unveiling solutions and implications for policy and health, *Atmospheric Environment: X*, 25, 100308,

https://doi.org/https://doi.org/10.1016/j.aeaoa.2024.100308, 2025.
Wang, C., Liggio, J., Wentzell, J. J. B., Jorga, S., Folkerson, A., and Abbatt, J. P. D.: Chloramines as an important photochemical source of chlorine atoms in the urban atmosphere, *Proceedings of the National Academy of Sciences*, 120, e2220889120, https://doi.org/doi:10.1073/pnas.2220889120, 2023.
Wang, T., Brown, S. S., Dubé, W. P., Tham, Y. J., Zha, Q., Xue, L., Poon, S., Wang, Z., Blake, D. R., Tsui, W., and Parrish, D. D.: Observations of nitryl chloride and modeling its source and effect on ozone in the planetary boundary layer of southern China, *Journal of Geophysical Research: Atmospheres*, 121, 2457-2475, https://doi.org/10.1002/2015jd024566, 2016.
Wang, X., Wang, H., Xue, L., Wang, T., Wang, L., Gu, R., Wang, W., Tham, Y. J., Wang, Z., Yang, L., Chen, J., and Wang, W.: Observations of N_2O_5 and $ClNO_2$ at a polluted urban surface site in North China: High N_2O_5 uptake coefficients and low $ClNO_2$ product yields, *Atmospheric Environment*, 156, 125-134, https://doi.org/10.1016/j.atmosenv.2017.02.035, 2017a.
Wang, Z., Wang, W., Tham, Y. J., Li, Q., Wang, H., Wen, L., Wang, X., and Wang, T.: Fast heterogeneous N2O5 uptake and ClNO2 production in power plant and industrial plumes observed in the nocturnal residual layer over the North China Plain, *Atmos. Chem. Phys.*, 17, 12361-12378, https://doi.org/10.5194/acp-17-12361-2017, 2017b.
Xia, M., Peng, X., Wang, W., Yu, C., Sun, P., Li, Y., Liu, Y., Xu, Z., Wang, Z., Xu, Z., Nie, W., Ding, A., and Wang, T.: Significant production of $ClNO_2$ and possible source of Cl_2 from N_2O_5 uptake at a suburban site in eastern China, *Atmospheric Chemistry and Physics*, 20, 6147-6158, https://doi.org/10.5194/acp-20-6147-2020, 2020.
Xia, M., Peng, X., Wang, W., Yu, C., Wang, Z., Tham, Y. J., Chen, J., Chen, H., Mu, Y., Zhang, C., Liu, P., Xue, L., Wang, X., Gao, J., Li, H., and Wang, T.: Winter $ClNO_2$ formation in the region of fresh anthropogenic emissions: seasonal variability and insights into daytime peaks in northern China, *Atmospheric Chemistry and Physics*, 21, 15985-16000, https://doi.org/10.5194/acp-21-15985-2021, 2021.
Xie, Y., Zhou, M., Hunt, K. M. R., and Mauzerall, D. L.: Recent PM2.5 air quality improvements in India benefited from meteorological variation, *Nature Sustainability*, https://doi.org/10.1038/s41893-024-01366-y, 2024.